Rare Metal Materials and Engineering
Volume 50, Issue 5, May 2021
Available online at www.rmme.ac.cn

Science Press

Cite this article as: Ahmad Farooq, Zhang Lin, Zheng Jun, et al. Microstructure and Corrosion Behavior of Duplex CrON Coatings in Molten Aluminum[J].Rare Metal Materials and Engineering, 2021, 50(05): 1523-1530.

ARTICLE

Microstructure and Corrosion Behavior of Duplex CrON Coatings in Molten Aluminum

Ahmad Farooq[1,2,3], Zhang Lin[1,2], Zheng Jun[1,2,3], Sidra Iram[1,2,3], Zhang Shihong[1,2,3]

[1] Key Laboratory of Green Fabrication and Surface Technology of Advanced Metal Materials (Anhui University of Technology), Ministry of Education, Maanshan 243002, China; [2] Research Center of Modern Surface & Interface Engineering, Anhui University of Technology, Maanshan 243002, China; [3] School of Materials Science and Engineering, Anhui University of Technology, Maanshan 243002, China

Abstract: The duplex CrON coatings were prepared on H13 tool steels by combination of plasma nitriding and arc ion plating. The effects of oxygen flow rate on microstructure and corrosion behavior of duplex CrON coating in the molten aluminum were investigated. Results show that the as-deposited coatings with oxygen flow rate of 0, 50, and 100 mL/min, namely CrON-0, CrON-50, and CrON-100 coatings, mainly consist of B1-CrN phase. The major components of CrON coating change from nitride into oxide phase with increasing the oxygen flow rate, and the Cr_2O_3 crystalline phase is obviously observed in the as-deposited coatings with oxygen flow rate of 200 mL/min, namely CrON-200 coating. Oxygen addition in nitride restrains the columnar growth of grains resulting in the dense microstructure. The surface defects and roughness increase with the increase of oxygen content. The failure behavior of duplex CrON coatings is mainly corrosion pitting in molten aluminium. The CrON-50 coating reveals the best corrosion resistance due to the dense columnar microstructure and high thermal stability. The dense Cr_2O_3 layer in CrON-200 coating is also favourable for corrosion protection against the molten aluminum.

Key words: CrON; duplex coating; microstructure; immersion corrosion; molten aluminum

In the aluminum die casting process, the die tool is subjected to severe operating conditions such as wear, corrosion, soldering and thermal fatigue[1]. Surface modification of the die tools, such as plasma nitriding and physical vapor deposition (PVD), has been used to improve the die life[2,3]. Die tools treated by plasma nitriding with proper stress and hardness gradients exhibit high wear and thermal fatigue resistance due to the nitrogen diffusion[4]. However, a great affinity between Al and Fe causes soldering through chemical/metallurgical reaction. PVD coatings as the effective diffusion barriers have been introduced to resist the molten aluminium attack. Further improvement can be achieved by the duplex treatment with a plasma nitriding layer beneath the PVD hard coating, which can be considered as the most appropriate treatment for die-casting tools[5,6].

Cr-based nitride coatings are preferred in die tool applications due to their superior oxidation resistance and chemical stability[7]. The Cr_2O_3/CrN bilayer coatings exhibit excellent thermal stability and good oxidation resistance than the single CrN coatings do, and these coatings are suitable for the die casting tools[8]. Because different gases are used during the deposition of nitride adhesion layer and oxide working layer, the application of oxide coating is more complicated, comparing to the application of nitride coatings. In addition, the thermal expansion coefficients are distinctly different between the oxide coating and steel substrate, resulting in the poor adhesion. The addition of the third element in the CrN coating has been investigated in several studies[9,10]. Hsu et al[11] reported the superior abrasion resistance and adhesion properties of Cr-O-N coating. Moreover, other researchers found that the CrN partially transforms into a passive Cr_2O_3 layer in the CrON coating, which improves the oxidation resistance at high temperature[12,13]. The oxynitride system has tunable properties with various microstructures by varying O/N in the coatings. Detailed information on CrON ternary oxynitride coatings was reported by the investigations[14-18]. However, there are few re-

Received date: May 09, 2020
Foundation item: Anhui Provincial Natural Science Foundation (2008085QE202); Anhui Provincial Key Research and Development Program (202004h07020020, 202004b11020011); Xijiang Innovation Team Project Funding of Zhaoqing
Corresponding author: Zhang Shihong, Ph. D., Professor, Key Laboratory of Green Fabrication and Surface Technology of Advanced Metal Materials (Anhui University of Technology), Ministry of Education, Maanshan 243002, P. R. China, Tel: 0086-555-2315289, E-mail: tougaoyouxiang206@163.com

ports about the corrosion resistance of CrON coatings in molten aluminum.

This work aims to explore the duplex CrON coating deposition and investigate its corrosion resistance against the molten A380 aluminum alloy. The pretreatment by plasma nitriding was conducted to increase the mechanical support for the oxynitride coatings under high cyclic thermal stresses. The arc ion plating system was employed to deposit CrN/CrON coatings on plasma nitrided AISI H13 tool steels. The CrN layer was deposited as a base layer, followed by a CrON top layer with different oxygen flow rates. The composition and microstructure were also reported.

1 Experiment

The CrN/CrON coatings were synthesized on plasma-treated AISI H13 tool steel substrates. The steel specimens were polished to reach the value of roughness (S_a) below 50 nm by diamond paste and subsequently cleaned with acetone and alcohol. The plasma nitriding was performed in a nitriding furnace. The gas mixture with V_{N_2}:V_{H_2}=1:3 and a total pressure of 200 Pa were maintained at 510 ℃ for 8 h. An industrial arc ion plating equipment with two Cr (purity of 99.99at%) targets installed symmetrically was utilized for coating deposition. Before the deposition, the base pressure of the chamber was less than 1×10^{-3} Pa, and the substrates were heated at 450 ℃. The specimens were cleaned through Ar^+ sputtering for 30 min at a substrate bias voltage of −300 V. The CrN base layer was deposited for 1 h in pure N_2 environment at a constant pressure of 3.5 Pa. The arc currents of Cr targets and the substrate bias were fixed at 120 A and −80 V, respectively. During the deposition of CrON top layer, oxygen gas was introduced into the chamber by varying the oxygen flow rate from 0 mL/min to 200 mL/min. The deposition time of CrON top layer was 1 h. The coatings treated by different oxygen flow rates of 0, 50, 100, and 200 mL/min were referred as CrON-0, CrON-50, CrON-100, and CrON-200, respectively. The total thickness of all coatings was around 5.3 μm.

The chemical composition and bonding position in the coating were characterized by X-ray photoelectron spectra (XPS). The phase structure of the coatings was analyzed using X-ray diffraction (XRD). A Raman spectrometer was used to characterize the bonding structure of the coating. The cross-sectional microstructure of the coating was analyzed by transmission electron microscope (TEM). TEM sample was prepared by a focused ion beam (FIB) system. The surface and cross-sectional morphologies were analyzed by a scanning electron microscope (SEM) and the surface roughness of all specimens was obtained by a KLA-Tencor P7 step profiler.

The thermal stability of the coatings was investigated after annealing at 700 °C. The coated specimens were simultaneously heated under an ambient air environment in a resistive furnace at 700 °C for 2 h. The temperature increased with the rate of 5 °C/min, holding at the target temperature for 2 h and subsequently cooling down to room temperature during the anneal process. The surface and cross-sectional morphologies of heat-treated specimens were observed by SEM.

The corrosion resistance of the CrON coating was evaluated through the static immersion test. The duplex coated AISI H13 steel pin specimens (Φ12 mm×100 mm) were used for the immersion test. Each experiment was carried out with A380 aluminum alloy of 1 kg in an alumina crucible at 700± 3 ℃. The experiment was performed for 1, 3, 5, and 7 h for each coating. After each immersion test, the residual solidified aluminium was removed by 10wt% NaOH solution and used to identify the damaged areas. The specimens were examined using an optical microscope (OM) and SEM. The corrosion pits area was measured by the percentage of areas covered with corrosion pits. The total observed area was 40 mm×20mm. The mass loss rate was evaluated after the immersion test by Eq.(1):

$$\text{Mass loss rate}=(W_0-W)/W_0\times100\% \quad (1)$$

where W_0 is the initial mass and W is the mass after immersion test.

2 Results and Discussion

2.1 Composition and morphology

The chemical composition of as-deposited CrON coatings with various oxygen flow rates in the deposition environment is presented in Table 1. The concentration of oxygen increases from 3.7at% to 52.4at% with increasing the oxygen flow rate from 0 mL/min to 200 mL/min, whereas the N concentration decreases from 44.3at% to 4.5at%. The Cr concentration also decreases, which can be related to the stronger affinity of oxygen with Cr than that of nitrogen with Cr[19]. The detection of a small amount of oxygen in the CrON-0 coating shows that the oxygen exists obviously in PVD coatings. It is possibly derived from the residual oxygen inside the deposition chamber and detection environment, as well as the thin oxide layer formed by exposure in the air[20].

The surface morphologies of as-deposited coatings and EDS spectra of the particles are presented in Fig.1. The particles and craters are observed on all coating surfaces, which are the typical characteristics of arc ion plating technique. And the particles mainly consist of metallic Cr ejected from the arc target, as the EDS spectrum shown in Fig.1a and 1d. The particle density on the coating surface reduces slightly with increasing the oxygen flow rate to 100 mL/min. It can be attributed to the target poisoning effect due to the formation of a thin layer of chromium oxide with higher melting point (above 2400 ℃)[21]. The further increase of oxygen flow rate during coating deposition increases the number of particles, as

Table 1 Composition and roughness of CrON coatings

Coating	O_2 flow rate/ mL·min^{-1}	Elemental composition/at%			Surface roughness, S_a/μm
		Cr	O	N	
CrON-0	0	52.0	3.7	44.3	0.187
CrON-50	50	48.4	18.1	34.5	0.216
CrON-100	100	45.9	40.5	13.6	0.277
CrON-200	200	43.1	52.4	4.5	0.356

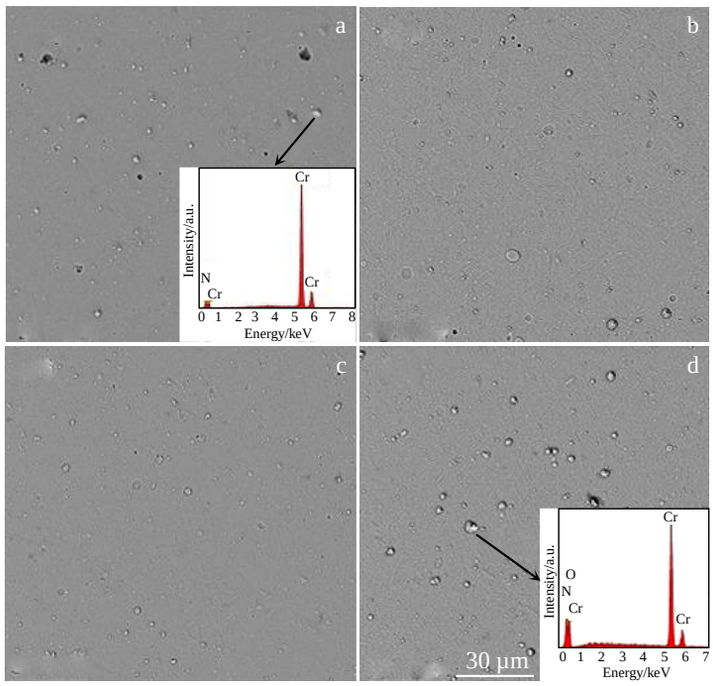

Fig.1 Surface morphologies of different as-deposited CrON coatings: (a) CrON-0, (b) CrON-50, (c) CrON-100, and (d) CrON-200

shown in Fig. 1d. A relatively higher concentration of oxygen can cause severe poisoning of Cr target and thereby reduce the electrical conductivity of the targets. The unstable arc spot on the target surface generates more droplets and increases the amount of macroparticles on the coating surface[22].

The surface roughness (S_a) of as-deposited coatings is summarized in Table 1. It can be seen that the surface roughness of the CrON coating increases with increasing the oxygen flow rate, which can be related to the increase of defects, such as particles or craters on the surface of coating. The cross-sectional morphologies of as-deposited coatings is presented in Fig. 2. It can be seen that the microstructure of the coatings

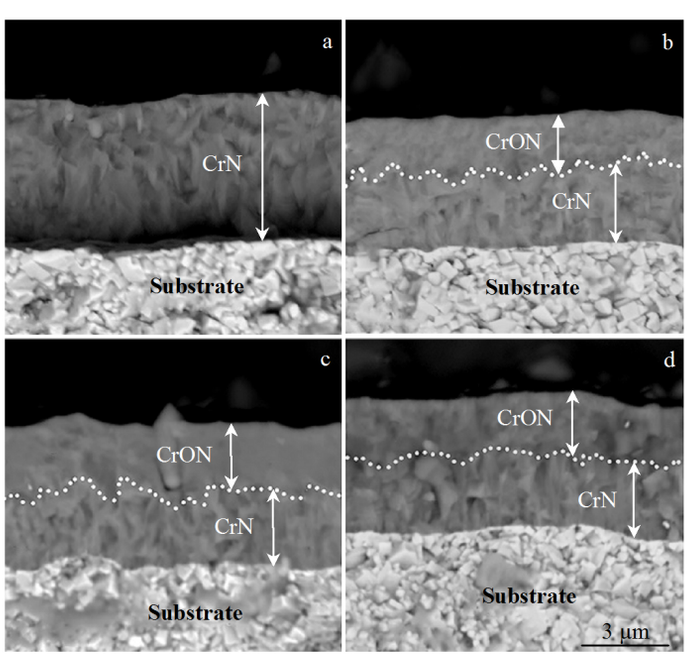

Fig.2 SEM images of cross-sectional morphologies of different as-deposited CrON coatings: (a) CrON-0, (b) CrON-50, (c) CrON-100, and (d) CrON-200

changes from a coarse columnar into a dense columnar with increasing the oxygen flow rate. It is clear that the grain size decreases with the increase of oxygen content of the coating, resulting in the microstructure change from the columnar into dense, and then featureless[12,14].

2.2 Microstructure analysis

The bonding status of CrON coatings is characterized through the binding energies by XPS spectra (Fig. 3). The peaks associated with Cr, O, N, and C elements are identified. All the spectra of CrON coatings are calibrated with C 1s peak at 284.8 eV[23]. Fig. 3 shows the Cr 2p spectra of different as-deposited CrON coatings. It consists of two strong peaks related to Cr $2p_{3/2}$ and Cr $2p_{1/2}$. The multiple split characteristics are considered for the detection of Cr (III) ionic state in Cr 2p spectra[23]. The fitting of Cr $2p_{3/2}$ confirms the characteristic peak of Cr-metal (573.5 eV) and Cr-N (574.4 eV)[24] and multiple splitting peaks of Cr-O bonds (575.7, 576.7, 577, and 578.9 eV)[23]. As the oxygen content increases, the Cr-N bonding fraction reduces from 60% to 12 %, whereas the Cr-O bonding fraction increases from 32% to 88%. The metallic Cr detected in the first sub-peak can be related to the existence of macroparticles on the coating surface[13]. The shift of binding energy towards the higher value confirms the increase of oxides with increasing the oxygen flow rate.

The XRD patterns of as-deposited CrON coatings with various oxygen flow rates are shown in Fig. 4. The diffraction peaks observed in CrON-O, CrON-50, and CrON-100 coatings can be related to the CrN phase. The additional peaks observed in CrON-200 coating are related to the Cr_2O_3 phase. It is important to mention that the diffraction peaks of CrN phase are also observed in CrON-200 coating. It is attributed to the nitride phase from the CrN base layer. In the case of CrON coatings deposited with low oxygen flow rates, no oxide phase is found in XRD analysis, although the high oxygen content (18.1at%) is detected in XPS analysis. The low-intensity band (2θ=33.5°) observed in CrON-100 coating maybe is attributed to the nano-crystalline Cr_2O_3 with an amorphous phase fraction.

With the addition of oxygen in CrN coating, the intensity and width of CrN (200) diffraction peak increase and subsequently decrease. Castaldi et al[12] reported the growth of (200) diffraction planes with increasing the oxygen content is attributed to the enhanced polarizability due to higher electronegativity of oxygen, which probably stabilizes the lower energy planes. Meanwhile, the further reduction can be related to the decrease of B1 phase and the growth of h-Cr_2O_3 oxide phase with higher oxygen content. Moreover, the reduction of CrN (200) diffraction peak intensity cannot be excluded due to the amorphization regardless of random orientation and more defective crystal structure. The slight shift of all diffraction patterns towards a lower angle is obvious in Cr-based coatings due to the variation in stress situations and solid solution phase formation[25,26].

The Raman spectra of as-deposited CrON coatings mainly consist of four bands, as shown in Fig. 5. The lower intensity bands at 302, 338, and 615 cm^{-1} are attributed to the normal Eg phonon modes, whereas the high-intensity band in the range of 535~555 cm^{-1} originates from A1g mode[27]. The lower intensity Eg band centered near 302, 338, and 615 cm^{-1} is common in both CrN and Cr_2O_3 structures[27,28]. The A1g characteristics band at 535 cm^{-1} in CrON-0 coating can be related to CrN structure[28]. A positive shift can be observed in this band with increasing the oxygen content. The A1g band at 555 cm^{-1} in CrON-200 coating can be related to the Cr_2O_3 bonding

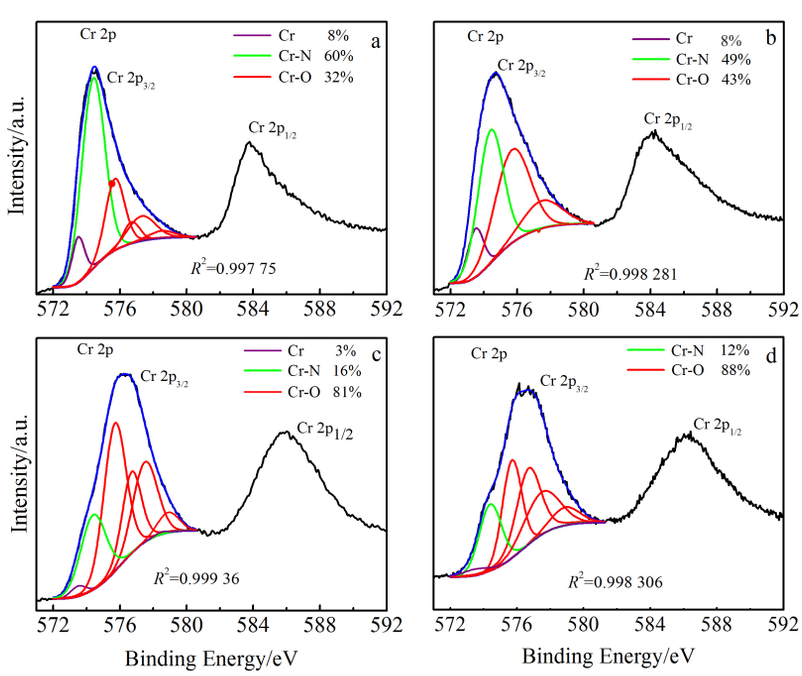

Fig.3 XPS spectra of Cr 2p of different as-deposited CrON coatings: (a) CrON-0, (b) CrON-50, (c) CrON-100, and (d) CrON-200

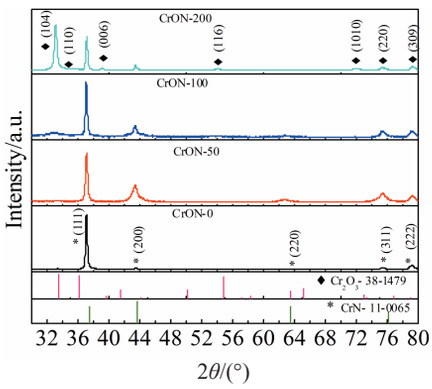

Fig.4 XRD patterns of different as-deposited CrON coatings

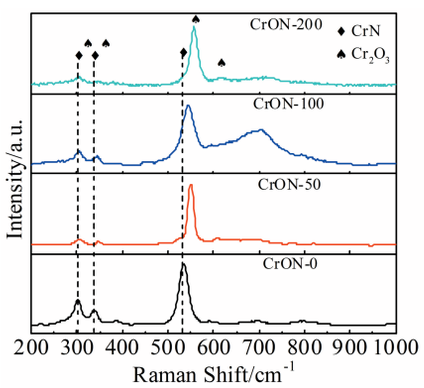

Fig.5 Raman spectra of different as-deposited CrON coatings

structure[28]. Similarly, the Raman spectra of CrON-50 and CrON-100 coatings show bands overlapping of CrN (535 cm^{-1}) and Cr_2O_3 (555 cm^{-1}) peaks, which confirms the presence of oxide bonding fraction. The additional wide band centered at 707 cm^{-1} in CrON-100 coating can be related to local site defects in CrN structure induced by oxygen. A similar vibration structure in Cr_2O_3 Raman spectra with a small fraction of impurities was observed by other researchers[29].

The microstructure is further characterized through TEM. Fig. 6 shows the high resolution transmission electron microscope (HRTEM) images and selected area electron diffraction (SAED) patterns of CrON-50 coating and CrN layer. There is an obvious transition from columnar to dense structure in Fig. 6a. A columnar structure with vertical growth extends through the thickness of the CrN base layers. While the columnar size and width reduce in the CrON layer, as shown in Fig.6a and 6b. The columnar grains in the CrN base layer extend through the entire layer, while the oxygen in CrON top layer hinders the columnar growth. The average width of columnar grains reduces from 374 nm to 113 nm in CrON top layer, which is consistent with the results in other studies[12,13]. The HRTEM/invert fast Fourier transformation (IFFT) images and SAED patterns obtained from CrN and CrON top layer are shown in Fig.6c and 6d, respectively. The grain size reduces with the introduction of oxygen. Fig. 6e and 6f show that the distinct spots in the SAED patterns of CrN layer are altered to the ring spots in the SAED patterns of CrON layer, reflecting the reduction of crystallinity in CrON coating with the introduction of oxygen. The SAED patterns from both layers also agree with the B1-NaCl CrN structure.

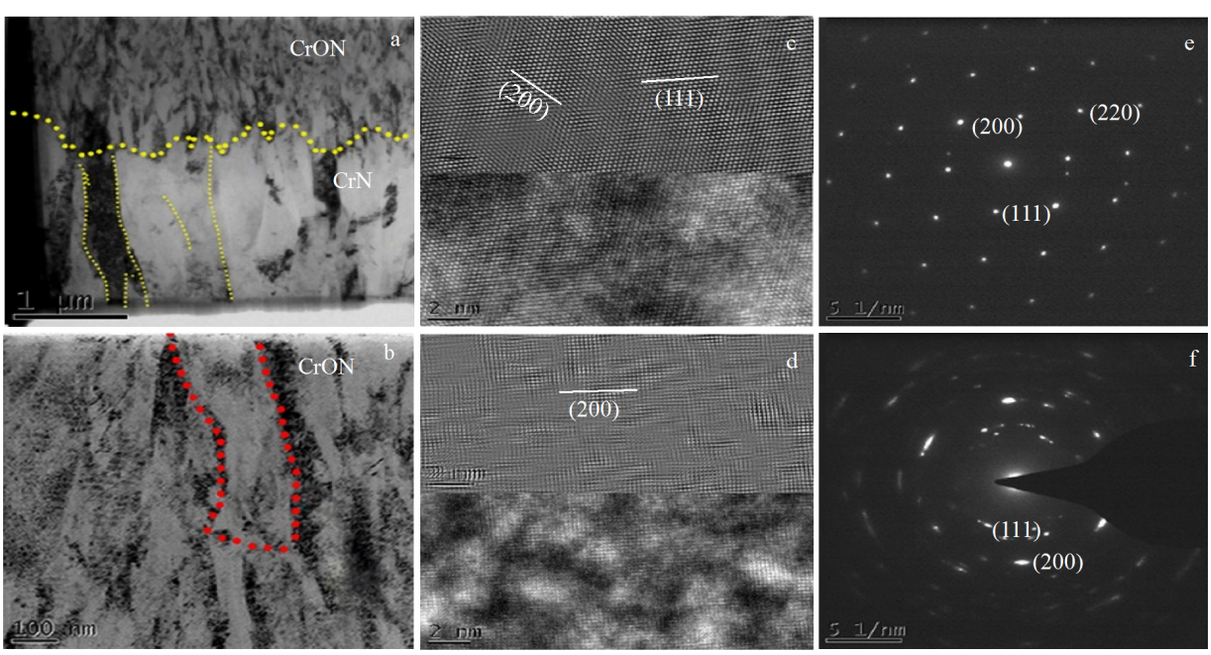

Fig.6 TEM images of CrN-50 coating (a) and CrON-50 layer (b); HRTEM/IFFT images of CrN (c) and CrON-50 (d) layers; SAED patterns of CrN (e) and CrON-50 (f) layers

2.3 Thermal stability

The thermal stability of the CrON coatings is evaluated after annealing at 700 ℃ for 2 h in an ambient atmosphere. The surface and cross-sectional morphologies after heat treatment are shown in Fig. 7. It can be seen that the CrON-100 coating has full oxidation with the obvious oxide layer from Fig. 7c and 7g. And some oxide meshes are observed on the surface of CrON-0 and CrON-100 coatings from Fig. 7a and 7c. The CrON-200 coating exhibits the best protection against the oxidation attack, as shown in Fig. 7d and 7h, which can be related to the dense Cr_2O_3 phase structure. The oxidation resistance of CrON/CrN bilayer coating at elevated temperature is better than that of the monolayer CrN coating[30]. The Cr_2O_3 top layer is ideal for oxidation protection[10,13].

2.4 Corrosion behavior in molten aluminum

Fig. 8 shows the images of duplex CrON coated AISI H13 steels after immersion in molten A380 aluminum alloy at 700 ℃ for 5 and 7 h. It can be seen that the surface of the coated steels is covered with corrosion pits after the immersion test. The CrON-50 and CrON-200 coatings exhibit fewer corrosion pits than other coatings do. It is also important to mention that all the specimens exhibit a similar corrosion behavior after immersion for 1, 3, 5 and 7 h. Localized corrosion pits appear on the surface of all pins, while there are no cracks observed in the CrON coatings.

The damage to the coated pins is evaluated by corrosion pits area and mass loss rate, as shown in Fig. 9. The CrON-50 and CrON-200 coated specimens exhibit the relatively lower corrosion pits area (<1.5%) and mass loss rate (<0.15%). The mass loss rate of the coated samples is probably attributed to two reasons[31]: (1) the aluminum diffusion to the matrix, resulting in the formation of Fe-Al-Si intermetallic phases between the molten aluminum and matrix; (2) the escape of Fe element from the matrix and the formation of Fe-Al-Si compounds at the interface during the immersion test process.

For CrON-50 coating, the dense columnar microstructure of oxynitride top layer provides an effective barrier than the nitride base layer does. Meanwhile, the lower surface defects at elevated temperature are favorable for corrosion resistance[32]. The CrON-200 coating exhibits a passive oxide top layer with dense Cr_2O_3 structure, which is contributed to the enhanced oxidation resistance at 700 ℃. Previous studies also reported that Cr_2O_3 is favorable to develop the corrosion resistance of steel[10,11]. However, the pitting corrosion is caused by the surface defects and metallic macroparticles. The CrON-0 and CrON-100 coatings exhibit larger corrosion pits area and mass loss rate after the immersion test. The CrON-0 nitride coating with poor thermal stability and wider columnar grain structure fails to provide sufficient resistance against the localized corrosion. Similarly, the CrON-100 coating with a porous oxide layer at high temperature also causes severe corrosion damages.

It is known that nitride coatings are not subjected to direct corrosion during the contact with molten aluminum[33]. After a short time (less than 3 h) of immersion corrosion, few corrosion pits can be seen on the coating surface, indicating that CrON coatings can inhibit the formation of Fe-Al-Si compounds[34]. However, the corrosion resistance decreases after the long time immersion test. It can be mainly related to the

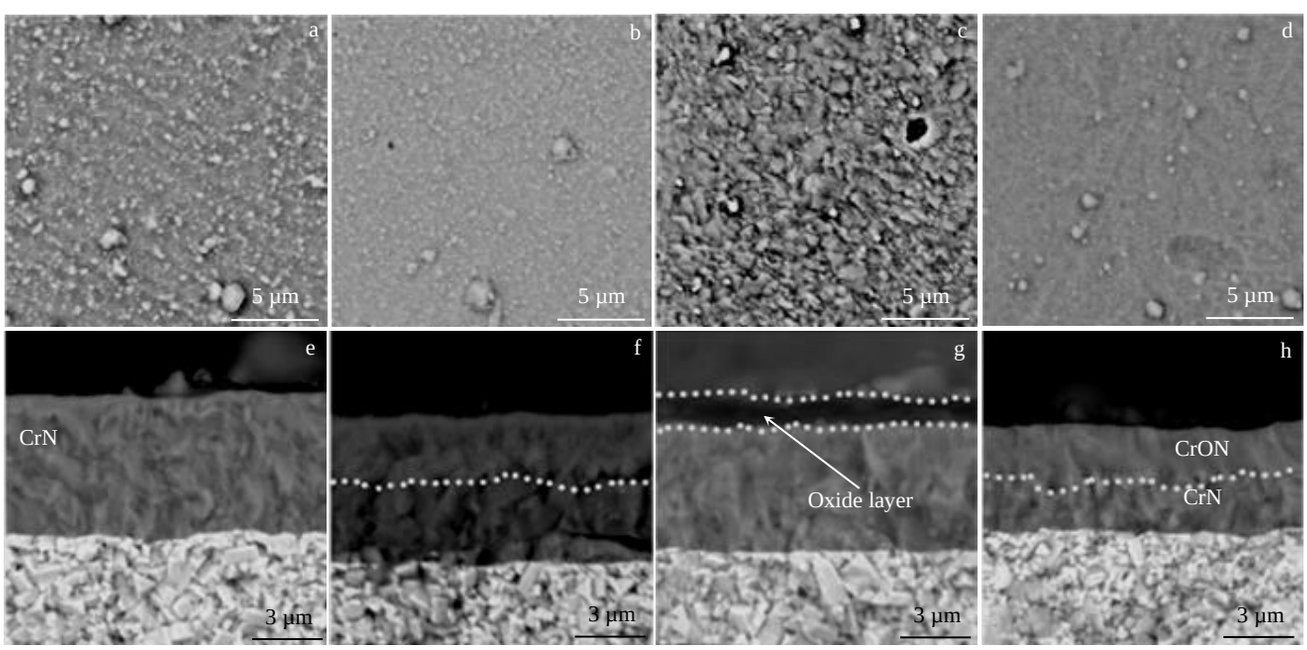

Fig.7 Surface (a~d) and cross-sectional (e~h) morphologies of different CrON coatings after annealing at 700 ℃ for 2 h: (a, e) CrON-0, (b, f) CrON-50, (c, g) CrON-100, and (d, h) CrON-200

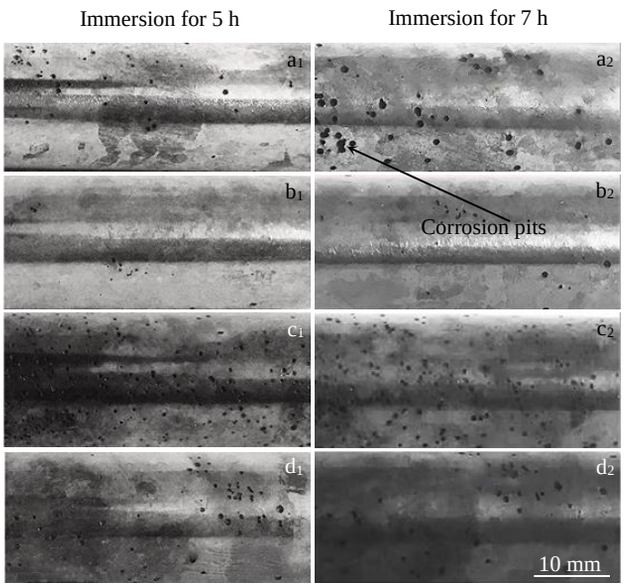

Fig.8 Macrographs of duplex CrON coated AISI H13 steels after immersion in molten aluminum at 700 °C for 5 h and 7 h: (a_1, a_2) CrON-0, (b_1, b_2) CrON-50, (c_1, c_2) CrON-100, and (d_1, d_2) CrON-200

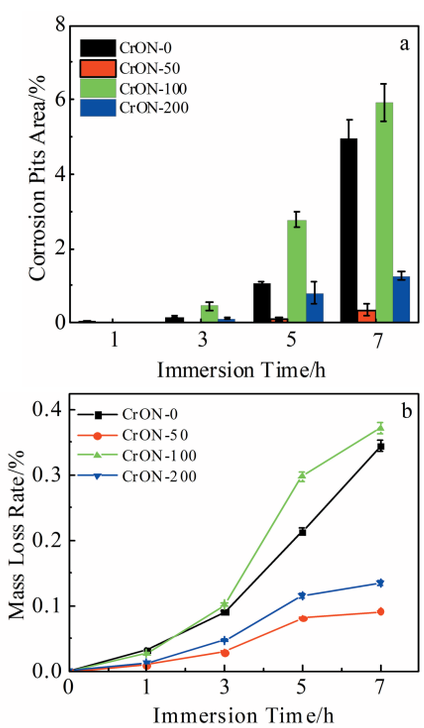

Fig.9 Corrosion pits area (a) and average mass loss rate (b) of different duplex CrON coatings on tool steels after immersion for 1, 3, 5, and 7 h

defects of the coatings. The growth defects, such as pinholes and macroparticles, provide initial diffusion path of aluminum alloy. The melt diffuses through the defects and forms Fe-Al-Si intermetallic compounds, which further deteriorates the coating layer from the substrate. In addition, the coarse columnar structure and loose oxide layer accelerate the diffusion of aluminum and iron elements at elevated temperature.

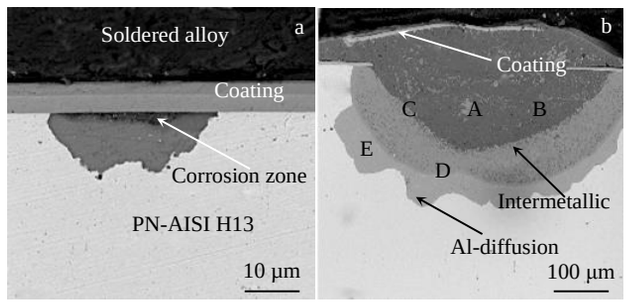

Fig.10 SEM images of cross-sectional morphologies of duplex CrON-50 coating after immersion for 7 h

Table 2 EDS analysis results of corrosion areas in Fig.10b

Corrosion area	Elemental composition/wt%				
	Al	Fe	Si	Cr	O
A-corrosion debris	69.3	17.9	7.8	1.2	3.1
B-alloy matrix	96.3	-	3.7	-	-
C-intermetallic	66.3	20.8	9.8	3.1	-
D-dense compound layer	59.4	28.6	10.0	2.0	-
E-alloy diffusion zone	54.0	40.5	3.4	2.1	-

Fig. 10 presents the cross-sectional morphologies of localized corrosion on CrON-50 coated steel specimen after immersion for 7 h. The corrosion pit is clearly observed beneath the CrON coating in Fig. 10a, indicating that the corrosion medium of melt is penetrated into the nitrided steel substrate. The severe corrosion attack is shown in Fig. 10b. The EDS analyses of the corrosion zone is concluded in Table 2. The A, B, C, D, and E areas in Fig. 10b represent the corrosion debris, alloy matrix, intermetallic layer, dense compound layer, and alloy diffusion zone, respectively. Nazari et al[35] reported the corrosion phenomena between the molten aluminum alloy and tool steel. The complex reaction layers are suggested as the intermetallic layer (Al_8Fe_2Si), dense compound layer (Al_5FeSi) and alloy diffusion zone ($Al_{12}Fe_5Si$). The composition of these phases is similar to the EDS results in Table 2.

3 Conclusions

1) The microstructure and corrosion behavior of the duplex CrON coatings are strongly influenced by oxygen content.

2) The columnar growth of nitride phase is restrained by the oxygen addition, and the structural evolution of CrON coatings from nitride to oxide phase is observed with increasing the oxygen flow rate.

3) The CrON coatings with oxygen flow rate of 50 and 200 mL/min reveal excellent corrosion resistance against the molten aluminum, which is attributed to the dense microstructure and high thermal stability.

References

1 Jhavar S, Paul C P, Jain N K. *Engineering Failure Analysis*[J], 2013, 34: 519
2 Chang S H, Lin Y K, Huang K T. *Surface and Coatings Technology*[J], 2012, 207: 571
3 Sokovic M, Panjan P, Kim R. *Journal of Materials Processing Technology*[J], 2004, 157-158: 613
4 Das K, Alphonsa J, Ghosh M *et al*. *Surfaces and Interfaces*[J], 2017, 8: 206
5 Peng J H, Zhu Z Z, Su D Y. *Tribology International*[J], 2019, 129: 232
6 Navinšek B, Panjan P, Gorenjak F. *Surface and Coatings Technology*[J], 2001, 137: 255
7 Chim Y C, Ding X Z, Zeng X T *et al*. *Thin Solid Films*[J], 2009, 517: 4845
8 Ho W Y, Huang D H, Huang L T *et al*. *Surface and Coatings Technology*[J], 2004, 177-178: 172
9 Ren Xingrun, Huang Zhu, Liu Meixia *et al*. *Rare Metal Materials and Engineering*[J], 2018, 47(4): 1100 (in Chinese)
10 Shao T, Ge F F, Dong Y *et al*. *Wear*[J], 2018, 416-417: 44
11 Hsu C H, Chen Y D. *Thin Solid Films*[J], 2009, 517: 1655
12 Castaldi L, Kurapov D, Reiter A *et al*. *Surface and Coatings Technology*[J], 2008, 203: 545
13 Ho W Y, Hsu C H, Huang D H *et al*. *Surface and Coatings Technology*[J], 2005, 200: 1303
14 Warcholinski B, Gilewicz A, Lupicka O *et al*. *Surface and Coatings Technology*[J], 2017, 309: 920
15 Suzuki K, Suematsu H, Thorogood G J *et al*. *Thin Solid Films* [J], 2017, 625: 111
16 Warcholinski B, Gilewicz A, Kuprin A S *et al*. *Vacuum*[J], 2018, 156: 97
17 Kuprin A S, Kuznetsova T A, Gilewicz A *et al*. *Problems of Atomic Science and Technology*[J], 2016, 106: 211
18 Li W Z, Yi D Q, Li Y Q *et al*. *Journal of Alloys and Compounds* [J], 2012, 518: 86
19 Minami T, Nishio S, Murata Y. *Surface and Coatings Technology* [J], 2014, 254: 402
20 Dobrzanski L A, Zukowska L W, Kubacki J *et al*. *Archives of Materials Science and Engineering*[J], 2008, 32: 99
21 Yun J S, Hong Y S, Kim K H. *Journal of the Korean Physical Society*[J], 2010, 57: 103
22 Ramm J, Neels A, Widrig B *et al*. *Surface and Coatings Technology*[J], 2010, 205: 1356
23 Biesinger M C, Payne B P, Grosvenor A P *et al*. *Applied Surface Science*[J], 2011, 257: 2717
24 Wang X B, Zhang X M, Li Q Y *et al*. *Solar Energy Materials and Solar Cells*[J], 2018, 188: 81
25 Suzuki T, Saito H, Hirai M *et al*. *Thin Solid Films*[J], 2002, 407: 118
26 Urgen M, Ezirmik V, Senel E *et al*. *Surface and Coatings Technology*[J], 2009, 203: 2272
27 Chen H Y, Lu F H. *Thin Solid Films*[J], 2006, 515: 2179
28 Barshilia H C, Rajam K S. *Journal of Materials Research*[J], 2004, 19: 3196
29 Fleischer K, Caffrey D, Farrell L *et al*. *Thin Solid Films*[J], 2015, 594: 245
30 Ho W Y, Shen C H, Chang C L *et al*. *Surface and Coatings Technology*[J], 2007, 202: 745
31 Chang S H, Huang K T, Wang Y H. *Materials Transactions*[J], 2012, 53: 745
32 Dinu M, Mouele E S M, Parau A C *et al*. *Coatings*[J], 2018, 8: 17
33 Molinari A, Pellizzari M, Straffelini G *et al*. *Surface and Coatings Technology*[J], 2000, 126: 31
34 Joshi V, Srivastava A, Shivpuri R. *Wear*[J], 2004, 256: 1232
35 Nazari K A, Shabestari S G. *Journal of Alloys and Compounds* [J], 2009, 478: 523

等离子渗镀CrON复合涂层结构与抗铝液熔蚀性能

Ahmad Farooq[1,2,3]，张　林[1,2]，郑　军[1,2,3]，Sidra Iram[1,2,3]，张世宏[1,2,3]

(1. 先进金属材料绿色制备与表面技术教育部重点实验室(安徽工业大学)，安徽 马鞍山 243002)

(2. 安徽工业大学 现代表界面工程研究中心，安徽 马鞍山 243002)

(3. 安徽工业大学 材料科学与工程学院，安徽 马鞍山 243002)

摘　要：采用等离子渗氮/电弧离子镀复合方法在H13模具钢表面制备出CrON涂层，研究氧流量对CrON复合涂层结构及抗铝液熔蚀性能的影响。结果表明，随着氧流量的增加，所制备的涂层主要物相由氮化物向氧化物转变，在氧流量较低时主要呈现面心立方CrN结构，而在氧流量为200 mL/min时制备的涂层形成典型的Cr_2O_3晶体相特征。掺入适量的氧，CrN涂层柱状晶生长受到抑制，涂层结构更加致密。涂层表面缺陷和粗糙度随着氧含量的增加而增大。CrON复合涂层在铝液中的失效形式是局部点蚀。由于形成致密的结构和良好的热稳定性，在氧流量为50 mL/min时制备的涂层具有优异的抗铝液熔蚀能力，而氧流量较高时表面生成致密的Cr_2O_3抗氧化层也有利于提高抗铝液熔蚀性能。

关键词：CrON；复合涂层；微观结构；热熔蚀；铝液

作者简介：Ahmad Farooq，男，1988年生，博士生，先进金属材料绿色制备与表面技术教育部重点实验室（安徽工业大学），安徽 马鞍山 243002，E-mail：mrfl24@yahoo.com